2012

Limited Thermal Conductance of Metal-Carbon Interfaces

Jaime J. Gengler
Air Force Research Laboratory

Sergei V. Shenogin
Air Force Research Laboratory

John E. Bultman
University of Dayton, jbultman1@udayton.edu

Ajit K. Roy
Air Force Research Laboratory

Andrey A. Voevodin
Air Force Research Laboratory

See next page for additional authors

Author(s)
Jaime J. Gengler, Sergei V. Shenogin, John E. Bultman, Ajit K. Roy, Andrey A. Voevodin, and Christopher Muratore

Limited thermal conductance of metal-carbon interfaces

Jamie J. Gengler,[1,2,a)] Sergei V. Shenogin,[1,3] John E. Bultman,[1,4] Ajit K. Roy,[1] Andrey A. Voevodin,[1] and Chris Muratore[1]

[1]*Air Force Research Laboratory, Materials and Manufacturing Directorate, Nanoelectronic Materials Branch, 2941 Hobson Way, Wright–Patterson Air Force Base, Ohio 45433, USA*
[2]*Spectral Energies, LLC, 5100 Springfield Street, Suite 301, Dayton, Ohio 45431, USA*
[3]*UES, Inc., 4401 Dayton—Xenia Rd., Dayton, Ohio 45432, USA*
[4]*University of Dayton Research Institute, 300 College Park, Dayton, Ohio 45469, USA*

(Received 29 August 2012; accepted 3 October 2012; published online 1 November 2012)

The thermal conductance for a series of metal-graphite interfaces has been experimentally measured with time-domain thermoreflectance (TDTR). For metals with Debye temperatures up to ~400 K, a linear relationship exists with the thermal conductance values. For metals with Debye temperatures in excess of ~400 K, the measured metal-graphite thermal conductance values remain constant near 60 MW m^{-2} K^{-1}. Titanium showed slightly higher conductance than aluminum, despite the closeness of atomic mass and Debye temperature for the two metals. Surface analysis was used to identify the presence of titanium carbide at the interface in contrast to the aluminum and gold-carbon interfaces (with no detectable carbide phases). It was also observed that air-cleaved graphite surfaces in contact with metals yielded slightly higher thermal conductance than graphite surfaces cleaved *in vacuo*. Examination of samples with scanning electron microscopy revealed that the lack of absorbed molecules on the graphite surface resulted in differences in transducer film morphology, thereby altering the interface conductance. Classical molecular dynamic simulations of metal-carbon nanotube thermal conductance values were calculated and compared to the TDTR results. The upper limit of metal-graphite thermal conductance is attributed to the decreased coupling at higher frequencies of the lighter metals studied, and to the decreased heat capacity for higher vibrational frequency modes. © *2012 American Institute of Physics*. [http://dx.doi.org/10.1063/1.4764006]

I. INTRODUCTION

Allotropes of carbon (e.g., fullerenes, nanotubes, and graphene) have been an intense subject of study for many years due to the fact that these materials have extraordinary physical properties. For example, the in-plane thermal conductivity of graphene (measured by Raman spectroscopy[1]) has recently been reported to be in the range 4840–5300 W m^{-1} K^{-1}. Another example is the longitudinal thermal conductivity of a single-wall carbon nanotube (measured by Joule self-heating[2]) reported as ~3500 W m^{-1} K^{-1} at room temperature. Such very high values of thermal conductivity make carbon-based materials attractive candidates for thermal management heat-sink applications. However, coupling heat into and out of carbon allotropes has been challenging since the interface thermal conductance between carbon and other materials can be quite low. For example, carbon nanotube-metal contacts have thermal interface conductance values less than 1 MW m^{-2} K^{-1} (as measured by a photoacoustic technique[3,4]). Another more promising example is metal-graphene contacts exhibiting thermal interface conductance values up to 80 MW m^{-2} K^{-1} (as measured by time-domain thermoreflectance (TDTR)[5,6]). The conductance upper limit was reported between aluminum and oxygen-functionalized graphene. However, these measurements are indirect since TDTR cannot resolve conductance effects from metal-graphene and graphene-substrate interfaces (due to the very small thickness of the graphene layer). In Refs. 5 and 6, it was assumed that these two graphene interface conductances acted in series. By fixing the graphene-silicon dioxide conductance to a value of ~100 MW m^{-2} K^{-1} (as determined by the 3ω method[7]), it became possible to extract the metal-graphene conductance values. Recently, Mak *et al.*[8] measured the graphene-silicon dioxide conductance by TDTR and reported a value of ~50 MW m^{-2} K^{-1}. Using this value would have altered the results of Refs. 5 and 6, so a more direct metal-carbon interface conductance measurement would be beneficial.

It has been shown that the room temperature behavior of a metallic thermal contact to that of the graphite basal plane is similar to that of the outer shell of a multi-walled carbon nanotube.[9] This provides a model representation of a hexagonal carbon-metal interface, which is more feasible for experimental studies and interpreting results with existing thermal conductance models. As a result, some experimental (TDTR) and theoretical work has been performed regarding the thermal conductance between metal and highly oriented pyrolitic graphite (HOPG) surfaces.[10–13] The work by Schmidt *et al.*[10] demonstrated that the thermal interface conductance between gold (Au), aluminum (Al), chromium (Cr), and titanium (Ti) with HOPG ranged from 30 to 120 MW m^{-2} K^{-1}. Application of a diffuse mismatch model (DMM) with a perfect interface assumption failed to explain

a)Author to whom correspondence should be addressed. Electronic mail: jamie.gengler.ctr@wpafb.af.mil.

these experimental results and it was concluded that contributions from interfacial roughness and chemistry may have been dominant. For further insight into interfacial state contributions, Smoyer *et al.*[12] prepared three samples of Au-coated HOPG by varying the HOPG surface treatment prior to metal deposition: as-cleaved in air, electron beam cleaned, and ion beam cleaned. The as-cleaved sample yielded the highest interface conductance at room temperature ($\sim$31 MW m^{-2} K^{-1}). This was hypothesized to originate from air impurities (e.g., water and hydrocarbons) that promoted reactivity between Au and HOPG. An electron beam cleaned sample was presumed to have removed such air impurities from the HOPG surface and the Au-HOPG interface conductance decreased to $\sim$24 MW m^{-2} K^{-1}. Finally, an ion beam cleaned sample was shown to have induced surface roughness of the HOPG surface and the measured Au-HOPG interface conductance dropped to $\sim$7 MW m^{-2} K^{-1}. It was suggested that inelastic phonon scattering processes needed to be incorporated into the DMM model in order to explain the observed conductances.

In this report, thermal interface conductance values are measured for Au, Cr, Ti, Al, copper (Cu), and tantalum (Ta) in contact with either air-cleaved or vacuum-cleaved HOPG surfaces. These metals were selected to represent a broad range of Debye temperatures (from 165 K for gold to 630 K for chromium). The experimental thermal conductance values are compared to molecular dynamics simulations of these metals in contact with sidewalls of carbon nanotubes, and the results are interpreted in terms of vibrational densities of states (DOS) as well as the physical characteristics of the metal-carbon interfaces.

II. EXPERIMENTAL PROCEDURE

HOPG substrates were obtained from SPI Corporation. These samples had dimensions of 10 mm $\times$ 10 mm $\times$ 1 mm and were characterized as "Grade 1." The grain size measured by Debye–Scherrer analysis of x-ray diffraction data was on the order of millimeters, with low mosaic spread which facilitates cleavage. HOPG substrates were cleaved by applying an adhesive strip and pulling the surface layers of graphite off to expose fresh layers in both laboratory air (approximately 25% relative humidity) and ultra high vacuum (UHV) (base pressure $<5\times10^{-9}$ Torr). Cleaved samples were transferred into a metal thin film processing chamber via a UHV load-lock equipped with a residual gas analyzer to monitor cleanliness of the transfer system. X-ray photoelectron spectroscopy (XPS) was used to characterize surface composition of air-cleaved and vacuum-cleaved HOPG (without exposure to air between cleaving and analysis). An XPS Kratos Ultra delay line detector spectrometer with monochromatic Al Kα radiation (hν = 1486.58 eV) was used in the study. Survey and high-resolution spectra were collected from a 700 $\times$ 400 μm^2 spot size at normal incidence with respect to the sample surface using fixed analyzer pass energies of 160 and 20 eV for the survey and high-resolution spectra, respectively. A charge neutralizer was not used due to good conductivity of all samples. Metal films were grown on both air-cleaved and vacuum-cleaved graphite surfaces by a high power pulsed magnetron sputtering process. The peak power density for each sputtering target was on the order of kilowatts per square centimeter as measured with a digital oscilloscope. There was some material dependence of the power; however the nominal power was the same for each target used. The power supply was operated at a frequency of 120 Hz and a pulse time of 90 μs. All substrates were grounded during metal deposition and were only naturally heated by the deposition process. An optical pyrometer reported maximum temperatures to be on the order of 55–70 °C. Metal film thicknesses ranged from 55 nm to 100 nm for the different metals. The metal film thicknesses were measured by electron probe microanalysis,[14] which is well suited for sample architectures composed of thin and chemically distinct layers. Film thicknesses were confirmed for a few selected samples with Rutherford backscattering measurements and picosecond acoustics from TDTR. Metal film thickness values from all three techniques agreed within approximately 3%.

Thermal conductance of the metal-HOPG interfaces was performed with a two color TDTR lab.[15] The output of a mode-locked Ti:sapphire laser is split into a pump and a probe beam. The pump beam ($\lambda\sim$785 nm) is sent first through a pulse compressor and then through an electro-optic modulator (EOM), which imposes a square-wave pulse train with a frequency of 9.8 MHz. The pump beam is then aligned along a mechanical translation stage to systematically alter the timing between the pump and the probe pulses. The probe beam is sent through the OPO for wavelength modification ($\lambda\sim$ 600 nm for use with Cu and $\lambda\sim$ 700 nm for use with all other metals). Both beams are then focused to a spot size of $\sim$50 μm diameter at a 45° angle to the sample. The reflected probe beam is spatially filtered, recollimated, and sent through a 750 nm short pass optical filter to reject scattered pump-beam light. Finally, the probe beam is passed through a neutral-density filter (optical density = 1.0) and focused onto a silicon photodiode detector. The output of the detector is sent to the input of a dual phase, radio frequency lock-in amplifier that has its reference channel connected to the same electronic signal that drives the EOM. The scans and data acquisition are computer controlled by means of a homemade LABVIEW program. TDTR data were acquired from five randomly chosen locations on each sample surface. Data analysis was performed with a nonlinear least squares application to Cahill's frequency domain model.[16] The only unknown variables were the metal-HOPG interface conductance and the HOPG thermal conductivity, and these parameters could be simultaneously determined. The results from the five scans of each sample were used to establish an average $\pm$ standard deviation value.

III. MOLECULAR DYNAMICS SIMULATIONS

The interfacial thermal conductance was evaluated using non-equilibrium molecular dynamics simulations. The models of (16, 16) multi-wall carbon nanotubes (MWCNT) were interfaced with atomic models of different metals (Al, Cu, Au, Ti, Cr, and Ta). The simulation box size ranged from 40 to 50 Å and contains 5200 to 8000 explicit atoms depending on the system (a sample snapshot is presented in Fig. 1). The

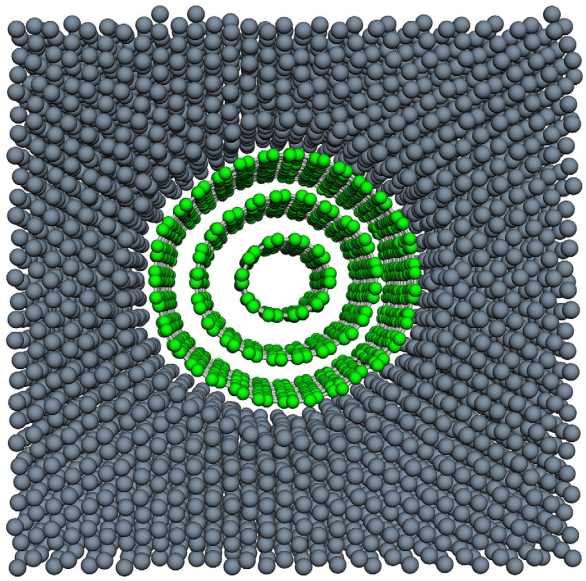

FIG. 1. Cross—section snapshot of the simulation model for MWCNT in aluminum.

atoms were interacting via the polymer consistent force field (PCFF) potential with an integration time step of 0.5 fs and 3D periodic boundary conditions used throughout the simulations. PCFF is a second generation force field derived from *ab initio* models and parameterized against a wide range of experimental observables for aromatic structures.[17,18] PCFF consolidates parameters for organic and inorganic materials.[19–21] The anharmonic corrections and energy cross-terms implemented in PCFF make it particularly suitable for simulations of thermal energy relaxation and thermal transport in nanostructures. Nanotubes were inserted in the void created in the bulk metal with the appropriate size and geometry. The final positions of metal atoms around the nanotubes were determined after a 1 ns MD equilibration run at standard temperature and pressure with the Nose-Hoover thermostat and the Parrinello-Rahman barostat, which allows all 3 dimensions and 3 angles of the simulation cell to relax independently of each other. After relaxation, the interface was defined as a cylinder (between carbon atoms and the first layer of metal atoms) drawn at a distance of 1.95 Å (i.e., the carbon van-der-Waals radius) from the outer nanotube shell. The interface area is determined by the nanotube radius and was independent of the metal to facilitate quantitative comparisons. Nanotubes embedded in metal were heated with constant power in the range 10–100 nW while the same cooling power was applied to metal atoms on the periphery of the cell to keep the total energy constant (i.e., the microcanonical ensemble). After 1 ns of equilibration, the radial temperature profile having cylindrical symmetry was plotted and steady-state temperature drops at the interface were measured. The conductance k of an interface with area A was calculated using the following equation:

$$k = \frac{\dot{Q}}{A\ \Delta T}, \tag{1}$$

where $\dot{Q}$ is heat flux and ΔT is the temperature drop at the interface. The ΔT vs. $\dot{Q}$ relationship is usually nonlinear as an indication that conductance increases with temperature. The conductance at a specified interface temperature (300 K) was evaluated after extrapolation of Eq. (1) to zero heating power using a quadratic fit.

IV. RESULTS AND DISCUSSION

The interface conductance values determined in this work are plotted in Fig. 2. The x-axis values are the ratio of the Debye temperatures of the metals[22] (165 K for Au, 240 K for Ta, 343 K for Cu, 420 K for Ti, 428 K for Al, and 630 K for Cr) to that of the c-axis Debye temperature for graphite[23] of 950 K. It is insightful to consider this relationship of Debye temperatures since a ratio of 1 would approximate an ideal interface. There are a few points worth mentioning about Fig. 2. First, there is a small but noticeable difference for each metal studied between the values obtained for vacuum-cleaved versus air-cleaved HOPG samples. The thermal interface conductance values for the air-cleaved samples are always slightly higher (10%–20%). This is in accord with the results of Ref. 12 where the implication was made that impurities in air should lead to increased reactivity between metals and HOPG. To further investigate the difference between air-cleaved and vacuum-cleaved HOPG samples, scanning electron microscopy (SEM) images were obtained for 10 nm of Au deposited on the two different substrates. The image displayed in Fig. 3(a) shows that the coverage of Au is uniform and complete for the air-cleaved sample. For the vacuum-cleaved HOPG sample in Fig. 3(b), there were some voids in Au film coverage. An image analysis had determined ~16% reduction in Au coverage due to porosity in the film. Such Au film morphology on the vacuum-cleaved sample results from Ehrlich-Schwoebel diffusion barriers developing at the edges of gold islands during film growth as reported for low temperature (<100 °C) gold growth on single crystal graphite.[24] Other metals investigated here showed similar, dendritic coverage patterns on the vacuum-cleaved HOPG substrate. These diffusion barriers in turn may qualitatively account for the ~10% decrease of interface thermal conductance for vacuum-

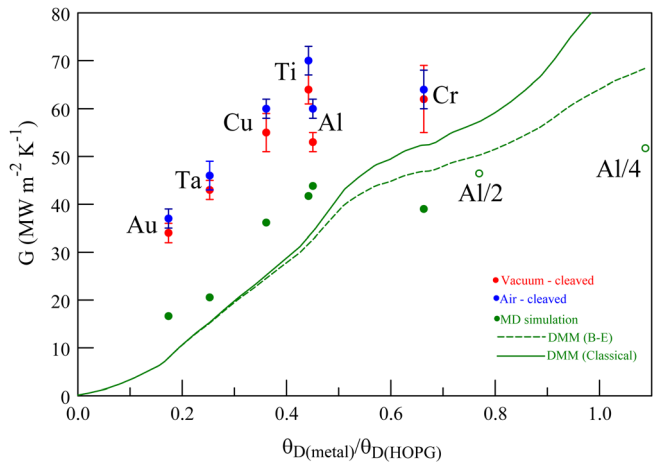

FIG. 2. Thermal interface conductance values plotted against Debye temperature ratios for the metal—HOPG samples studied. Results from molecular dynamics simulations for the metal—MWCNT system and DMM calculations are included for comparison.

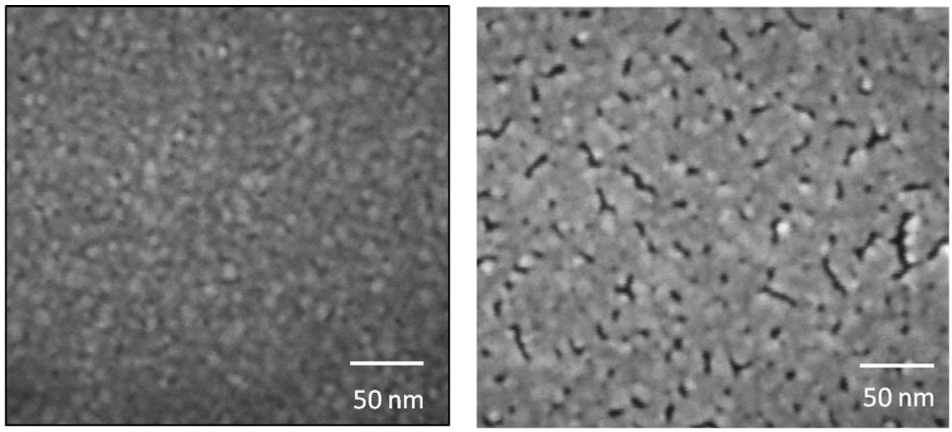

FIG. 3. SEM images of 10 nm Au deposited on (a) air—cleaved and (b) vacuum—cleaved HOPG substrates.

cleaved versus air-cleaved HOPG samples with the various metals.

Second, from the Fig. 2 data comparison, it is apparent that the experimental results were approximately 15–30 MW m^{-2} K^{-1} larger than the theoretical values. Since only phonon scattering mechanisms are theoretically taken into account in the simulations, it is hypothesized that there is also an electromagnetic contribution to the experimental thermal interface conductance.[25,26] For example, there have been reports on "charge mirroring" effects at metallic interfaces, where unscreened metal ion potentials and interaction of surface plasmons can contribute to the overall thermal conductance.[27,28] The possibility of such enhanced thermal coupling in metal-HOPG interfaces results from electromagnetic interactions between surface plasmons in the metal and transient dipoles in graphite. The graphite dipoles are created by thermally fluctuating carbon atoms, which create an in-plane electric current known as Johnson–Nyquist thermal noise. A recent detailed analysis[29] shows that this electromagnetic contribution for thermal interface conductance between metal-graphite interfaces is ~22 MW m^{-2} K^{-1}, which closely matches the difference between the experimental and theoretical values reported here.

It was observed that experimental measurements of conductance for titanium and chromium in Fig. 2 deviated most significantly from simulation results. These metals have the highest thermodynamic driving force for carbide formation based on comparison of Gibbs free energy values. An XPS investigation of interfacial carbide formation was conducted where films of titanium with 6 nm thickness were grown on HOPG under conditions identical to those used to produce the Ti-HOPG sample characterized in Fig. 2. This 6 nm thickness was selected as it was estimated to be the maximum allowable thickness that would not completely inhibit escape of photoelectrons from the metal-carbon interface to the free surface for detection by the analyzer. The depositions were performed at the different temperatures or metal ion fluxes (which was altered by changing the way power was modulated to the sputtering target) required to produce a range of carbide layer thicknesses. Fig. 4 shows a shift in binding energy indicative of carbide formation[30] for samples processed at different temperatures and metal ion/metal atom flux ratios (J_i/J_a). As the intensity of the TiC peak increases, suggesting an increase in thickness of the carbide layer, the thermal conductance was observed to decrease in the range of conditions examined here. Future studies on carbide layer thickness and conductance will be conducted to quantify thickness with photoelectron intensity and examine a broader range of thicknesses under the same J_i/J_a ratios. This will allow examination of potential effects to ion damage at the interface (although initial studies showed that J_i/J_a must be reduced to avoid carbide formation). Fig. 4(b) shows the expected interface for the Ti-HOPG sample characterized in Fig. 2. If thickness is indeed correlated to intensity, chromium formed thicker carbide layers at lower temperatures compared to titanium. The presence of these carbide layers is likely a contributing factor of larger deviation from simulation results, which assumed perfect metal-carbon interfaces with only van der Waals interactions.

Finally, regarding Fig. 2, it can be seen that at an x-axis value of ~0.4 there is a "leveling off" effect of measured conductance values. In other words, metals that have a higher Debye temperature than ~400 K do not necessarily provide a higher metal-HOPG interface conductance (contrary to the aforementioned assumption regarding the Debye temperature ratios). A possible explanation for this is that the maximum vibrational frequencies in metals are typically less than 10 THz, whereas the maximum vibrational frequency in graphite is in excess of 45 THz.[13] This aspect is illustrated in Fig. 5 where density of states plots from MD simulations for the metals and MWCNT are shown. The "leveling off" effect of interface conductance is also reflected in the MD results and the change in slopes of the DMM curves. This trend is attributed to two simultaneous effects that result in weaker thermal coupling between vibrational modes with frequencies more than 10 THz. According to the diffuse mismatch model, the thermal interface conductance is proportional to the integral of the spectral heat capacity $C(T,\omega)$ multiplied by the DOS (for the metal and the MWCNT) and by the frequency-dependent coupling function $\chi(T,\omega)$ (averaged over all polarizations)

$$G(T) \propto \int_0^\infty C(T,\omega)\,\chi(T,\omega)\,DOS_{MWCNT}(\omega)\,DOS_{metal}(\omega)\,d\omega. \quad (2)$$

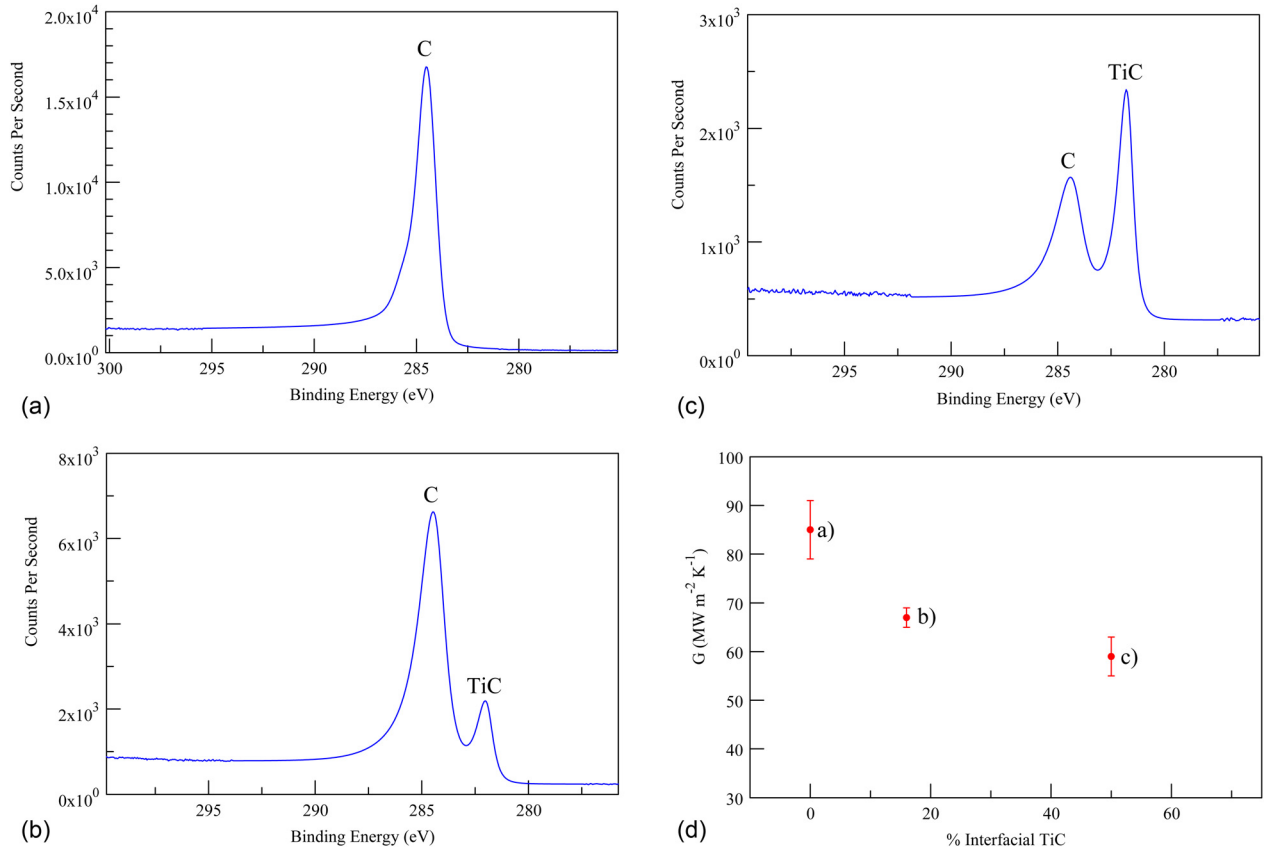

FIG. 4. X-ray photoelectron spectroscopy results for thin titanium films deposited on HOPG at (a) 22 °C; low J_i/J_a, Ar, (b) 22 °C; high J_i/J_a, and (c) 550 °C; high J_i/J_a. (d) Thermal conductance values for samples processed under the same three conditions with thicker Ti film for use as a TDTR transducer layer. The spectrum shown in (b) is representative of the interface present in the Ti-HOPG sample characterized in Fig. 2.

The increase of G with temperature, observed both in experiments[10] and in classical MD simulations,[29] must be attributed to an increase of the coupling function $\chi(\omega)$ at higher temperatures (due to anharmonically vibrating atoms). The temperature effect of Bose–Einstein heat capacity resulting in the temperature dependence of experimental values for G is rather weak at frequencies below 10 THz (which is the vibrational DOS overlap range for all considered metals excluding Cr). Therefore, the magnitude of interfacial conductance is dictated by the amplitude and the geometry of classical atom vibrations at the interface as governed by $\chi(\omega)$. Comparing MD results with evaluations of Eq. (2) with $\chi(\omega) = \text{constant}$ and $C(\omega) = \text{constant}$ (classical limit), plotted as the solid line in Fig. 2, one can conclude that the $\chi(\omega)$ is approximately constant within the first peak of the MWCNT vibrational spectrum (below 10 THz, see Fig. 5) and decreases at higher frequencies. This decrease in $\chi(\omega)$ results in a much lower value of G for the Cr-carbon interface calculated in MD simulations (39 MW m^{-2} K^{-1}, about 90% the conductance of the Al-carbon interface). We propose that such a decrease in G is caused by a very high elastic modulus of Cr and, therefore, much weaker anharmonic coupling between vibrational modes at a given temperature. To support this statement, we performed auxiliary simulations of metal composed of artificial Al atoms with half and quarter of the normal mass but normal interaction parameters. The results (plotted using extracted MD Debye frequencies as hollow circles in Fig. 2) indicate that if the stiffness is comparable, the conductance increases with Debye frequency even above 10 THz, although at a lower rate because of different oscillation geometry. However, for materials with much higher stiffness, the amplitude of atom vibrations is smaller, resulting in much weaker coupling of atomic vibrations across the Cr-carbon interface. This is confirmed by experimental results for Cr showing no increase of conductance in comparison with Al (see Fig. 2).

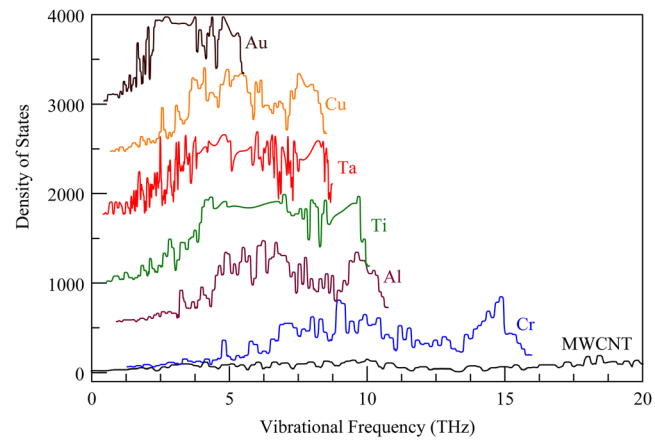

FIG. 5. Vibrational density of states results from the MD simulations for several metals and for MWCNT. The plots are offset for clarity.

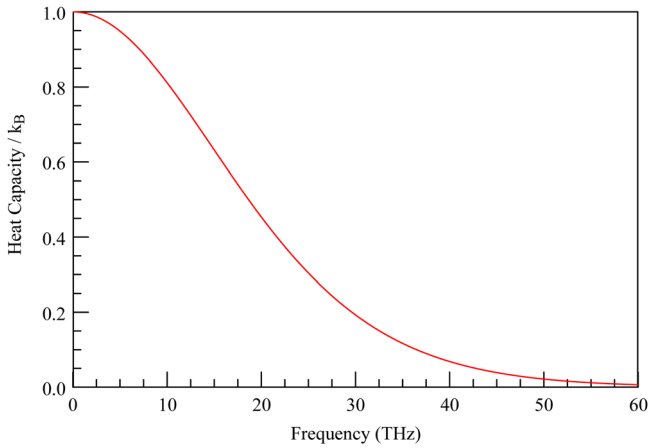

FIG. 6. Graphical representation of the Bose–Einstein heat capacity.

From a practical perspective, there is one more reason why the use of metals with Debye frequency higher than that of Al does not improve metal-HOPG conductance. The Bose–Einstein heat capacity of the vibrational modes decreases at room temperature for frequencies above 10 THz (see Fig. 6).

$$C(\omega,T)=\frac{(h\omega/kT)^2 e^{(h\omega/k_BT)}}{\left[e^{(h\omega/k_BT)}-1\right]^2}. \quad (3)$$

In Eq. (3), ω is the vibrational frequency, k_B is Boltzmann's constant, and T is temperature. The result of Eq. (2) with quantum heat capacity (Eq. (3)) is plotted in Fig. 2 as a dashed line, providing comparison with the classical result (solid line).

V. CONCLUSIONS

The thermal interface conductance between several metals and graphite has been measured by TDTR. All graphite samples cleaved in air had 10%–20% higher metal-carbon conductance values than those cleaved in vacuum, which has been correlated with metal deposition surface morphology patterns as demonstrated by SEM image analysis. All performed MD simulations had provided lower interface conductance than experimental values, and this offset is attributed to an electrostatic contribution to the thermal interface conductance. The metal deposition parameters controlling carbide formation for Ti and Cr interfaces with HOPG were explored along with their influence on metal-HOPG conductance values. Carbide layer formation was detected for higher energy thin film growth conditions and correlated with a reduction of thermal conductance. Lighter metals with Debye temperatures >400 K do not display enhanced thermal conductance with graphite due to decreased coupling and heat capacity of the higher frequency modes of vibration.

ACKNOWLEDGMENTS

The authors express thanks to the Air Force Office of Scientific Research for funding through the Low Density Materials Program, Grant FA8650-09-D-5307. We are also grateful for thin film thickness analyses performed by Ivan Petrov and Brandon Howe (Rutherford Backscattering Facility at the University of Illinois at Urbana-Champaign) and by Jared Shank and Fred Meisenkothen (electron probe microanalysis at Air Force Research Laboratory Materials Characterization Facility).

[1]A. A. Balandin, S. Ghosh, W. Bao, I. Calizo, D. Teweldebrhan, F. Miao, and C. N. Lau, Nano Lett. **8**, 902 (2008).
[2]E. Pop, D. Mann, Q. Wang, K. Goodson, and H. Dai, Nano Lett. **6**, 96 (2006).
[3]B. A. Cola, X. Xu, and T. S. Fisher, Appl. Phys. Lett. **90**, 093513 (2007).
[4]R. Cross, B. A. Cola, T. S. Fisher, X. Xu, K. Gall, and S. Graham, Nanotechnology **21**, 445705 (2010).
[5]Y. K. Koh, M.-H. Bae, D. G. Cahill, and E. Pop, Nano Lett. **10**, 4363 (2010).
[6]P. E. Hopkins, M. Baraket, E. V. Barnat, T. E. Beecham, S. P. Kearney, J. C. Duda, J. T. Robinson, and S. G. Walton, Nano Lett. **12**, 590 (2012).
[7]Z. Chen, W. Jang, W. Bao, C. N. Lau, and C. Dames, Appl. Phys. Lett. **95**, 161910 (2009).
[8]K. F. Mak, C. H. Lui, and T. F. Heinz, Appl. Phys. Lett. **97**, 221904 (2010).
[9]R. Prasher, Phys. Rev. B. **77**, 075424 (2008).
[10]A. J. Schmidt, K. C. Collins, A. J. Minnich, and G. Chen, J. Appl. Phys. **107**, 104907 (2010).
[11]J. C. Duda, P. E. Hopkins, T. E. Beechem, J. L. Smoyer, and P. M. Norris, Superlattices Microstruct. **47**, 550 (2010).
[12]J. L. Smoyer, J. C. Duda, P. M. Norris, and A. W. Lichtenberger, in *Proceedings of the ASME/JSME 2011 8th Thermal Engineering Joint Conference*, March 13-17, Honolulu, Hawaii, USA, AJTEC2011-44333 (2011).
[13]P. M. Norris, J. L. Smoyer, J. C. Duda, and P. E. Hopkins, J. Heat Transfer **134**, 020910 (2012).
[14]C. S. Campos, E. A. Coleoni, J. C. Trincavelli, J. Kaschny, R. Hubbler, M. R. F. Soares, and M. A. Z. Vasconcellos, X–Ray Spectrom. **30**, 253 (2001).
[15]J. J. Gengler, S. Roy, J. G. Jones, and J. R. Gord, Meas. Sci. Technol. **23**, 055205 (2012).
[16]D. G. Cahill, Rev. Sci. Instrum. **75**, 5119 (2004).
[17]H. Sun, J. Comput. Chem. **15**, 752 (1994).
[18]H. Sun, S. Mumby, J. R. Maple, and A. T. Hagler, J. Am. Chem. Soc. **116**, 2978 (1994).
[19]H. Sun, Macromolecules **28**, 701 (1995).
[20]H. Sun and D. Rigby, Spectrochim. Acta A **53**, 1301 (1997).
[21]H. Sun, J. Phys. Chem. B **102**, 7338 (1998).
[22]C. Kittel, in *Introduction to Solid State Physics*, 8th ed., edited by S. Johnson (Wiley, 2005), p. 116.
[23]J. Krumhansl and H. Brooks, J. Chem. Phys. **21**, 1663 (1953).
[24]R. Anton and I. Schneidereit, Phys. Rev. B **58**, 13874 (1998).
[25]G. D. Mahan, Phys. Rev. B **79**, 075408 (2009).
[26]G. D. Mahan, Phys. Rev. B **81**, 195318 (2010).
[27]I. Altfeder, A. A. Voevodin, and A. K. Roy, Phys. Rev. Lett. **105**, 166101 (2010).
[28]A. M. Nemilentsau and S. V. Rotkin, ASC Nano **6**, 4298 (2012).
[29]S. Shenogin, J. Gengler, A. Roy, A. Voevodin, and C. Muratore, "Molecular dynamics studies of thermal boundary resistance at carbon-metal interfaces," Appl. Phys. Lett. (Submitted).
[30]Q. Ma and R. A. Rosenberg, Phys. Rev. B **60**, 2827 (1999).